Magnetoencephalography With Optically Pumped He-4 Magnetometers at Ambient Temperature

Etienne Labyt, Marie-Constance Corsi, William Fourcault, Augustin Palacios Laloy, Francois Bertrand, Francois Lenouvel, Gilles Cauffet, Matthieu Le Prado, Francois Berger, Sophie Morales

▶ **To cite this version:**

Etienne Labyt, Marie-Constance Corsi, William Fourcault, Augustin Palacios Laloy, Francois Bertrand, et al.. Magnetoencephalography With Optically Pumped He-4 Magnetometers at Ambient Temperature. IEEE Transactions on Medical Imaging, 2019, 38 (1), pp.90-98. 10.1109/TMI.2018.2856367 . hal-02350924

HAL Id: hal-02350924
https://hal.science/hal-02350924

Submitted on 18 Nov 2019

HAL is a multi-disciplinary open access archive for the deposit and dissemination of scientific research documents, whether they are published or not. The documents may come from teaching and research institutions in France or abroad, or from public or private research centers.

L'archive ouverte pluridisciplinaire **HAL**, est destinée au dépôt et à la diffusion de documents scientifiques de niveau recherche, publiés ou non, émanant des établissements d'enseignement et de recherche français ou étrangers, des laboratoires publics ou privés.

Magnetoencephalography with optically pumped ^{4}He magnetometers at ambient temperature

Etienne Labyt*, Marie-Constance Corsi, William Fourcault, Augustin Palacios Laloy, François Bertrand, François Lenouvel, Gilles Cauffet, Matthieu Le Prado, François Berger, and Sophie Morales

***Abstract*— In this paper, we present the first proof of concept confirming the possibility to record magnetoencephalographic (MEG) signals with Optically Pumped Magnetometers (OPMs) based on the parametric resonance of ^{4}He atoms. The main advantage of this kind of OPM is the possibility to provide a tri-axis vector measurement of the magnetic field at room-temperature (the ^{4}He vapor is neither cooled nor heated). The sensor achieves a sensitivity of 210 fT/√Hz in the bandwidth [2 Hz - 300 Hz]. MEG simulation studies with a brain phantom were cross-validated with real MEG measurements on a healthy subject. For both studies, MEG signal was recorded consecutively with OPMs and Superconducting Quantum Interference Devices (SQUIDs) used as reference sensors. For healthy subject MEG recordings, three MEG proofs of concept were carried out: auditory and visual evoked fields (AEF, VEF), and spontaneous activity. M100 peaks have been detected on evoked responses recorded by both OPMs and SQUIDs with no significant difference in latency. Concerning spontaneous activity, an attenuation of the signal power between 8-12 Hz (alpha band) related to eyes opening has been observed with OPM similarly to SQUID. All these results confirm that the room temperature vector ^{4}He OPMs can record MEG signals and provide reliable information on brain activity.**

***Index Terms*— Optically pumped magnetometer, Helium 4, room temperature, vector measurement, magnetoencephalography, auditory evoked field, visual evoked field, spontaneous activity.**

I. Introduction

MAGNETOENCEPHALOGRAPHY (MEG) is a non-invasive functional imaging technique which consists in measuring the magnetic fields generated by the brain, about one billion times smaller than the Earth's magnetic field. Its high temporal resolution in the order of the millisecond gives the possibility of an online observation of brain activity [1]. Within the main clinical applications, the use of MEG, in combination with stereoelectroencephalography (SEEG), led to a localization of 50 to 80 % of the epileptogenic sources [2]-[5] and has demonstrated its usefulness in epilepsy presurgical evaluation [6][7]. MEG is also used in cognitive science to identify electrophysiological markers of brain activity in adults [8]-[10] and in children [11]. Novel potential clinical indications of MEG are also progressively emerging from clinical research, based on the investigation of resting state functional connectivity. In particular, MEG appears very promising for the management and diagnosis of dementia (mild cognitive impairment and Alzheimer's disease) [12]-[15], Parkinson's disease [16]-[18], traumatic brain injury [19]-[21] and multiple sclerosis [22]-[24].

Currently, MEG recordings rely on ultrasensitive Superconducting Quantum Interference Devices (SQUIDs) characterized by a magnetic sensitivity around 5 fT/√Hz (bandwith going from DC to 1.6 kHz on current Elekta machines: https://www.elekta.com/diagnostic-solutions/elekta-neuromag-triux/#triux-ar). However, wide dissemination of MEG systems is hindered by some limitations of commercial SQUIDs that require cryogenics and a bulky magnetically shielded room, leading to a cost close to 3M€ over 7 years (including the shielding cost). In this context, for ten years, new cryogenic-free sensors have emerged in the medical field: the optically pumped magnetometers (OPMs). To date only Spin Exchange Relaxation Free (SERF) optically pumped magnetometers have been used to measure MEG signals [25-28]. Sensitivities reported by these four research teams during recordings on healthy subjects, were 200 fT/√Hz from 5 to 150 Hz [25], 3.5fT/√Hz between 10 and 100 Hz [26], 21 fT/√Hz at 10 Hz [27] and 10 fT/√Hz above 1 Hz [28] for various sizes of cells and different alkali atoms. All these studies have been performed with one sensor but Romalis' team reported a multi-channel configuration based on a matrix of photodetectors. Last technical progresses have centered on developing individual, fiber-coupled modules (FC-OPMs). Single-channel [29] and multichannel [30]-[32] vapor-cell devices, as well as single-channel chip-scale modules [25] [33], have been demonstrated.

Nevertheless the spin exchange relaxation regime can only be reached by operating the sensor at a near-zero magnetic field with sufficiently high alkali metal density. As a result, the alkali vapor must be heated between 150 and 200°C and so, alkali SERF OPMs require thermal insulation increasing sensor distance to source. The dynamic range of alkali SERF OPMs is also limited by the width of the resonance of alkali atoms. Bandwidths and related sensitivities reported in previous alkali OPMs MEG recordings [25-28], cited above show the trade-off which has to be found between these both parameters. In one of these studies [27], bandwidth was even tuned in order to fit the frequency of alpha brain activity. Although recent technical advances trended to improve this issue [34] [35], sensitivities and bandwidths reported in these studies were only based on laboratory measurements and have not been applied to MEG measurements.

In the case of ^{4}He OPMs used in the current work, the ^{4}He vapor does not require neither being heated nor cooled, the sensor is operated at room-temperature and can be in contact with the skin. The distance between the sensor and the subject is thus reduced, resulting in an increase of the signal strength. The bandwidth of the sensor used ranged from 0.1 to 300 Hz. We have demonstrated that our ^{4}He OPMs could be used to

record magnetocardiographic signals and to provide reliable information about cardiac activity [36].

In this paper, the operability of our parametric ^{4}He OPMs for MEG measurement is demonstrated with a phantom and a healthy subject. Both measurements were cross validated with SQUID recordings. For the first time, three MEG experiments including auditory and visual evoked fields as well as spontaneous activity have been carried out at room temperature in a clinical environment.

II. Material

A. Principle of operation

Our sensor is an optically pumped magnetometer based on the parametric resonances of 4He metastable atoms in a near-zero magnetic field [37]–[39] (Fig 1). The 4He cell size was 1 cm x 1 cm x 1 cm. A detailed description of the sensor can be found in a previous publication [36].

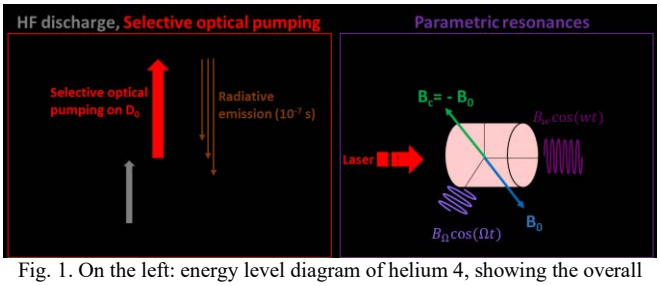

Fig. 1. On the left: energy level diagram of helium 4, showing the overall effect of the discharge and of the optical pumping. On the right: main elements of the parametric resonance magnetometer used in this work: a pump laser (which also acts as probe) goes through the cell and is photodetected. Two RF fields are applied along X and Y axes orthogonal axes yielding double parametric resonance. The external magnetic field $\boldsymbol{B_0}$ measured in this way is compensated by an opposite field $\boldsymbol{B_c}$.

A High frequency (HF) discharge at 32 MHz, coupled with circular electrodes of 5 mm radius and consuming 20 mW power, excites ^{4}He atoms from the fundamental state to the metastable one which is split by the static magnetic field into three Zeeman sublevels. At thermal equilibrium, Zeeman sublevels are almost equally populated and no significant absorption of the pump light is observed at resonance. A selective optical pumping (with a linearly polarized beam tuned on the D_0 line at 1083 nm) is thus performed to amplify the resonance signal by inducing a dissymmetry of the Zeeman-sublevel populations.

At low magnetic field, resonant variations of the absorbed light (of the same laser used for pumping) are detected when a static magnetic field is swept around the zero-field value (Hanle effect). Resonance can also be induced by an amplitude modulated magnetic field obtained by adding a radio-frequency (RF) field in the direction of the field to be measured. In our OPMs, in order to derive a vector measurement of the three components of the magnetic field, resonance is excited by two RF fields $B_\Omega \cos\Omega t$ and $B_\omega \cos\omega t$. These RF magnetic fields (respectively applied along the X and Y axes) are orthogonal to each other and to the direction of the polarization of the pump laser beam. Thanks to this detection scheme first introduced by Dupont-Roc and coworkers[40], three resonance signals are detected on the transmitted pump light at Ω, ω, and $\Omega \pm \omega$. To first order, the amplitude of each resonance is respectively proportional to one of the three components of the magnetic field to be measured (respectively B_x, B_y, and B_z). So, our ^{4}He OPM is the first sensor, to our knowledge, to be able to measure the three magnetic field components

The system is operated in a closed-control-loop system: the magnetometer is locked on the zero-magnetic field condition by applying a compensation magnetic field that cancels the ambient magnetic field. The value and direction of the measured magnetic field is deduced from the current injected in the compensation coil. This closed-loop mode of operation reduces the crosstalk between axes [37], [40]-[42].

B. Experimental set-up and sensor characterization

A gradiometer setup with two magnetometers is used during the experiments, as shown in Fig. 2. The first sensor, called OPM_1, is placed close to the subject's head. The second one, called OPM_2, is placed 30 cm away from the first one (far from the subject's head), and is used as a reference channel. This setup clearly differs from classical SQUID gradiometry with a baseline of 3-8 cm such as gradiometer present in the Elekta MEG machine.

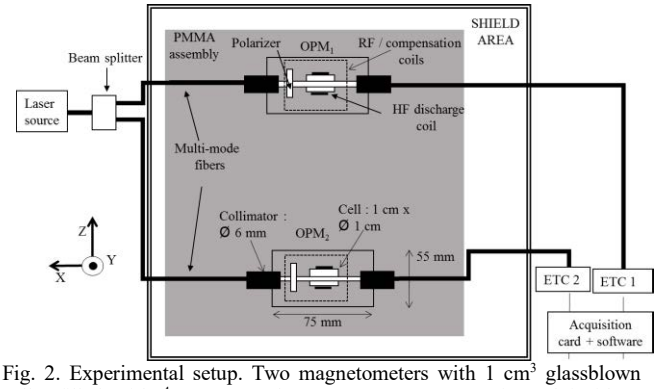

Fig. 2. Experimental setup. Two magnetometers with 1 cm^3 glassblown cells, filled with ^{4}He are used. Measurements are performed inside a magnetically shielded room. Horizontality of the setup was guaranteed by a house made polymethyl methacrylate (PMMA) holder. The bold line represents optical connections whereas the thin one corresponds to electrical connection. ETC stands for Electronic Treatment Card.

In laboratory environment (inside a 5-layered magnetically shield room), the measured sensitivity of a single sensor is of 210 fT/√Hz between 2 Hz and 300 Hz (Fig 3).

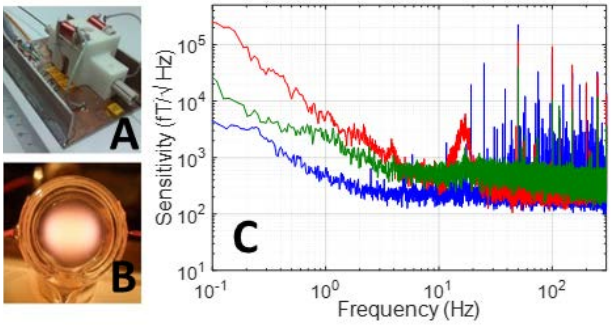

Fig. 3. Picture of the OPM without its cover (A); of the glassbown ^{4}He cell (B). Measured sensitivity (C) of a 4He magnetometer for laboratory (blue) and clinical environments with one sensor configuration (red) and gradiometer configuration (green). The bandwidth is 300 Hz

Sensitivity in clinical environment is somewhat deteriorated at low frequency due to magnetic disturbances induced by the building ventilation.

III. Method

MEG experiments have been carried out in a clinical environment at Clinatec (Grenoble, France), inside the magnetically shielded room dedicated to MEG measurements. For both OPMs and SQUIDs recordings, the active compensation of the magnetically shielded room (MaxShield® ; see https://ecatalog.elekta.com/neuroscience/content/pdf/NM23251B%20MaxShield%20datasheet.pdf) was used.

A. Simulated MEG recordings with a brain phantom

Operability of the ^{4}He OPMs is first demonstrated with simulated signals generated with the precision-engineered head phantom from Elekta. This head dry phantom contains 32 current dipoles. The phantom is based on the mathematical fact that an equilateral triangular line current produces equivalent magnetic field distribution to that of a tangential current dipole in a spherical conductor, provided that the vertex of the triangle and the origin of the conducting sphere coincide [43]. The phantom dipoles are energized using an internal signal generator to get a dipole moment of 12.7 nAm.

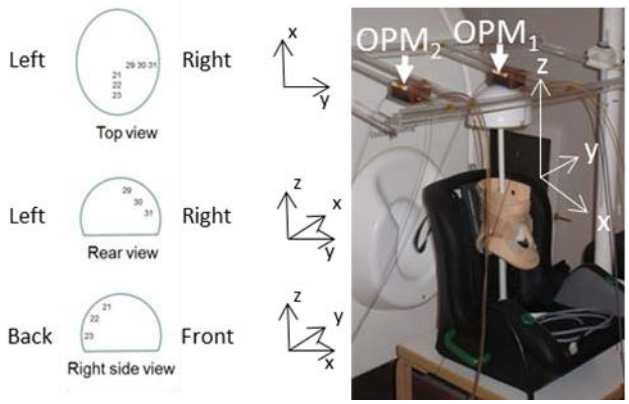

Fig. 4. Tests performed with the Elekta phantom. On the left, the spatial distribution of the dipoles within the volume of the phantom, and on the right, the tested configuration.

As shown in Fig 4, the optically pumped magnetometers rely on a non-magnetic holder to ensure the axes of the two magnetometers are parallel.. The OPM which measures the signal of interest (i.e. OPM_1) is placed at the vertex of the phantom, directly in contact with the surface. OPMs record the variations of the magnetic field along the X and Y axes while SQUID magnetometer taken as reference only measures magnetic field along Y axis (Z axis in the Elekta coordinate system).

Two experiments are carried out. In the first one, we test if our OPM is able to detect the signals emitted sequentially by several dipoles distributed within the whole volume of the phantom. The goal here was to test the robustness of our OPM sensor to distance source-sensor as well as to various source orientations. Given the geometry of the phantom, it is possible to work with only 6 dipoles (numbered 21, 22, 23 and 29, 30, 31) distributed within a quarter of the volume (Fig 5). The distance between the sensor and the dipole 29 is of 22 mm whereas the dipole 31 and the sensor are 45 mm away from each other. Each dipole along the radius of the phantom is oriented normally to the phantom surface. So, each dipole has a different orientation. Inter-Stimulus Interval (ISI) was set to 120 ms, close to the alpha rhythm frequency. The duration of each set of stimuli is of 80 ms. Selective filters are used in order to remove DC components and power line noise and a filter bank centered to 8.33 Hz (according to the frequency of excitation of the current dipole) and its harmonics was applied (Fig 5). .

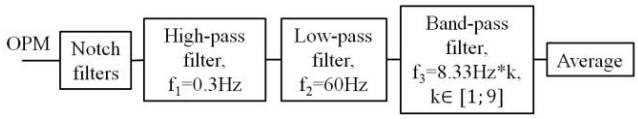

Fig. 5. Signal processing circuit applied in the experiment about OPM robustness to sensor-source distance (experiment 1). Notch filters were used to remove power line disturbance at 50 Hz and at its harmonics as well as DC components.

In the second experiment, only the dipole 29 is used. A comparison is made between signals successively detected by the OPM and by the SQUID sensor of the Elekta MEG system located at the nearest position of the dipole, i.e. the vertex. Recording time is set to 10 minutes. In this section, ISI was set to 346 ms. Each set of stimuli lasts 101 ms. OPM and SQUIDs recordings are synchronized on the phantom's stimulation signal. For OPM as well as SQUID sensor, a baseline time window preceding the dipole excitation is used to remove the DC offset (Fig 6).

Fig. 6. Signal processing circuit (SPC) applied in the experiment about influence of averaging time window (experiment 2).

Before averaging, SQUIDs data are processed with signal space separation method [44] in order to remove cross-talk effect and parasitic magnetic noise. Statistical OPM/SQUID comparison of averaged signals is performed with Spearman correlation coefficient.

B. MEG recordings with a healthy subject

Following successful measurements on a brain phantom, real MEG measurements in a healthy subject (male, 46 years old) were carried out in the frame of the clinical research protocol MAP_EFNI 2013-A00414-411 authorized by the French National Agency for drug Safety ANSM (Agence Nationale de Sécurité du Médicament et des produits de santé), and ethical committee. For this cross validation with real MEG signals, data were successively recorded with our OPM device and then, with the MEG machine (Elekta Vectorview Neuromag® 306 channels). Signal from one SQUID sensor (magnetometer) was selected as reference signal for comparison to OPM signal. The selected SQUID

sensor was still the nearest of the OPM location according to the experiment (see below). All recordings were performed with a sampling frequency of 1024 Hz and a bandwidth of [0.1; 330 Hz]. Three types of recordings have been performed as described below.

Fig. 7: Experimental setup used during Auditory Evoked Fields (AEFs) (left part), Visual Evoked Fields (VEFs) and alpha rhythm recordings (right part) carried out with OPMs

1) Auditory evoked fields, AEFs

a) Protocol

In this experiment, a binaural stimulus is applied to the subject with MEG compatible earphones (ER-10B from Etymotics®; see https://www.etymotic.com/auditory-research/microphones/er-10b.html). Stimulus duration is set to 100 ms. The auditory stimulus (70 dB beep at a frequency of 1 kHz) is emitted with a 750 ms periodicity. During MEG recordings, the subject is in the supine position, on his right side, on the MEG bed. Typical recording length was about 5 minutes. When OPMs were used, OPM_1 was placed over the left temporal area (Fig 7), regarding to T4 EEG electrode placement with respect to the 10-20 EEG system. It measures the MEG signal of interest and the background magnetic noise field B_R. Distance between OPM_1 and the head is set to the smaller value that avoids any contact between skin and the sensor. It is estimated to be 5 mm in average. OPM_2, located at about 30 cm away from OPM_1, and not above the subject's head, only measures B_R.

The aim of this test is to check if our device is able to detect AEFs, and more specifically, M100 peak (magnetic correlate of the N100 waveform in Auditory Evoked Potentials – AEP – in EEG). For that purpose, a comparison is made between the latencies (i.e interval of time between the stimulus and the most prominent brain magnetic signature, here the M100 peak) determined from averaged MEG signals successively recorded by OPMs and SQUIDs, through several sessions.

b) Applied signal processing methods

SQUIDs

Bad channels and periods contaminated by artifacts are first identified and labeled by automatic detection as well as visual inspection. Signal Space Separation (SSS)[44] is then applied in order to reduce the noise in MEG data and remove cross-talk effects. Epochs from 300 ms before the auditory stimulus (baseline window) to 300 ms after are extracted. Bad trials, contaminated by artifacts, are rejected. Selected epochs are averaged and filtered with a Finite Impulse Response (FIR) bandpass filter between 0.05 and 45 Hz. All these processing steps are performed using the software Brainstorm® [45].

OPM

In the case of MEG recordings performed by OPMs, Independent Components Analysis, through the FastICA method [46] [47], is applied to recorded signals (X and Y signals from each OPM). This method - commonly implemented in MEG - enables to separate components mainly corresponding to brain signal from component mainly corresponding to noise and artifacts [48], [49]. This separation can be easily done based on spectral content of each component. ICA was used rather than first order gradiometer due to the distance (30 cm) between our both OPM sensors. The last signal processing steps are performed with Brainstorm®, namely, epochs slicing (-300 ; + 300 ms with respect to the auditory stimulus), identification of the epochs contaminated by residual artifacts (performed through visual inspection), averaging of the selected epochs and finally, filtering with a FIR bandpass filter between 0.05 and 45 Hz.

c) AEF - Data analysis

In order to cross validate OPM recordings, OPM signals are compared to the signal recorded by a temporal SQUID magnetometer on which the largest AEF was observed. Statistical OPM/SQUID comparison of averaged signals is performed with Spearman correlation coefficient. M100 latencies - measured with the OPM and the SQUID - are also statistically compared with an equivalence test, namely with the two one-sided tests procedure [50] performed on the same number of epochs.

2) Visual evoked fields, VEFs

a) Protocol

Flashing white disc was displayed on a screen in front of the subject. The flashing white disc display duration was set to 150 ms and inter-stimulus time interval was set to 1067 ms. The screen was placed at the subject's focal distance, according to his/her visual acuity. The subject was seated on the MEG chair and was asked to keep eyes open. Typical recording length was about 5 minutes. During the experiment, OPM_1 is placed over the left occipital area, regarding to O1 EEG electrode placement in the 10-20 EEG system (see Fig. 8). It measures the MEG signal of interest and the residual field B_R. As in the previous experimental setup, distance between OPM_1 cell surface and the head is set to the smaller value that avoids any contact between skin and the sensor. It is estimated to be 5 mm in average (due essentially to the mechanics of the sensor, further improvements should allow to reduce it under 1 mm). OPM_2, located at about 30 cm away from OPM_1, and not above the subject's head, only measures B_R. As AEFs, the purpose of this experiment was to test the possibility to detect the M100 peak (magnetic correlate of the P100 waveform in visual evoked potential) associated to VEFs with our OPMs.

b) Applied signal processing methods and data analysis

For SQUIDs and OPM recordings respectively, signal processing steps and data analysis were the same as those applied for AEFs, excepted epoch duration which starts - 300 ms before and ends 450 ms after the visual stimulus.

3) Induced activity measured by the OPMs

a) Protocol

In this experiment, subject is asked to open or close his eyes every 20 seconds. Tempo is given by an auditory stimulus (beep sound). Each acquisition lasts between 5 and 7 minutes, to avoid tiredness of the healthy volunteer. The aim of this experiment is to detect the brain signal power modulation induced by eyes opening. OPMs placement was the same as for VEFs.

b) Applied signal processing methods

SQUIDs

Recordings were first post-processed with SSS [43] after identifying bad channels and periods contaminated by artifacts. Epochs from 2.5 seconds before to 2.5 seconds after the beep sound were extracted. Bad trials were rejected. For each trial, time-frequency analysis was performed with a Morlet-wavelet transforms (1 Hz frequency resolution) with 1/f power compensation (edge effects were excluded) in the alpha frequency band (8-12 Hz) and then, averaged. A z-score normalization was computed.

OPM

The recorded signal is first processed with fast ICA method to extract brain activity component. The next signal processing steps are performed with Brainstorm®: epochs slicing (- 2.5 s ; + 2.5 s with respect to the beep sound), rejection of trials contaminated by artifacts, time-frequency analysis performed with a Morlet-wavelet transforms (1 Hz frequency resolution) with 1/f power compensation (edge effects were excluded) in the alpha frequency band (8-12 Hz) and averaging. Finally, Z-score normalization was performed.

IV. Results

A. Simulated MEG signals from a brain phantom

1) Detection of the signal from any dipoles of the brain phantom

As shown in Fig 8, our vector ^{4}He OPM is able to measure signals generated by any dipole located within the whole volume of the phantom. Furthermore, simultaneously measurements along X and Y axes are possible.

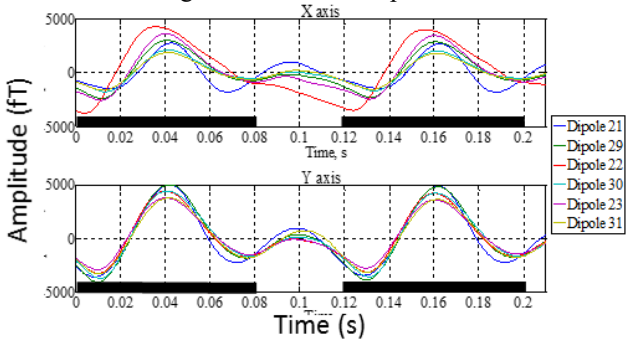

Fig. 8. Averaged signals obtained with OPMs along the X and Y axes with the 6 tested dipoles, which were successively excited. Dark bars correspond to dipole excitation period

2) Comparison between SQUIDs and OPM for a given dipole of the brain phantom:

Two comparison parameters are studied here: a) the general morphology/periodicity of the simulated signal as respectively recorded by the OPM and the SQUID; b) the influence of the time window used for averaging.

a) Morphology/periodicity

Spearman correlation between SQUID and OPM averaged data was computed for the Y axis (common to OPM and SQUID sensor). Along the Y axis, the Spearman correlation between the averaged signal obtained from OPM and SQUID is 0.97 for a 5 minutes recording time.

b) Influence of the averaging time window

Secondly, the time window used for averaging the OPM data was successively reduced and compared to averaged SQUID signal for 5 minutes (around 900 averages), used as reference (Fig 9). Spearman correlation was computed for each case and the limit correlation value was set to 0.75. Results recorded using OPMs revealed that a dipole signal should still reliably be observed along the Y axis with a time window of 30 s (correlation value at 0.78 - around 80 averages), whereas the limit for the X axis is higher than 90 s (around 250 averages). This difference can be explained by the smaller amplitude of the measured signal in this direction (due to phantom design, the signal of interest is mainly aligned along the Y axis). Along this Y axis, for a 30 s recording time, the Spearman correlation between the averaged signal obtained from OPM and SQUID was 0.78. Thus, this test evidences that synchronous signals with a statistically correlated envelope are obtained with our ^{4}He OPM with respect to SQUID magnetometer. Furthermore, a reduced recording time until 30 seconds can be considered with our OPMs.

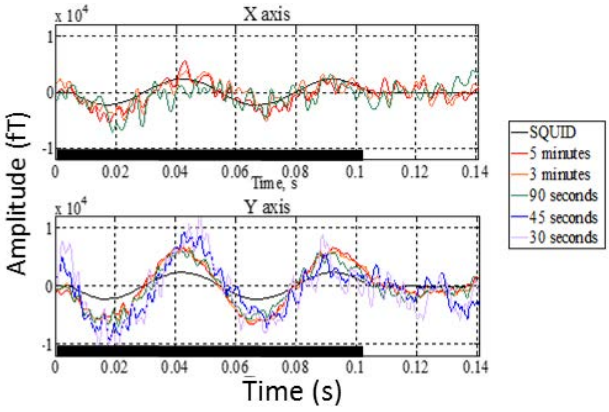

Fig. 9. Averaged signals obtained for different durations of the same phantom signal recorded by the OPMs along X and Y axes. Epochs of 140 ms were used. The dipole excitation period corresponds to the dark bar. Averaged SQUID signal, on 5 minutes recording (along Y axis only), is used as a reference. Averaged SQUID signal (dark curve) recorded along Y axis is reported on X axis graph only for comparison of signal periodicity The selected SQUID sensor is located at the nearest position of the vertex. In the case of the OPM, the observed fast oscillations are explained by the absence of a low-pass filter. This choice was made to reduce the potential sources of distortions and phase rotations which could induce variability in the signal periodicity.

These preliminary results obtained with a brain phantom validate the possibility to record simulated MEG signals with our ^{4}He OPMs at room temperature from X and Y axes.

B. MEG recordings on a healthy subject

1) Auditory evoked fields - AEF

As shown in Figure 10, M100 peak (the most prominent magnetic signature of the cerebral AEF response) can be observed from SQUIDs recordings at a latency of 100.3 ms after the stimulus onset, with a classical topography. This M100 peak was also found at a similar latency (100.6 ms) latency with the OPM placed over the temporal area.

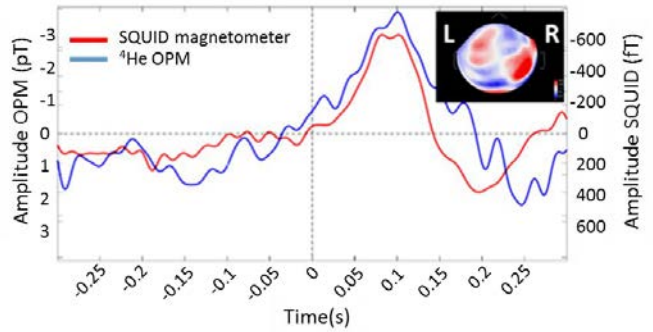

Fig.10. Averaged AEF on a healthy subject: Topography of AEF as recorded in MEG with the averaged signal over 38 epochs obtained from one SQUID sensor (magnetometer) placed in the right temporal area and averaged signals over 83 epochs obtained from our OPMs sensor.

In order to test the equivalence of M100 latencies distribution between OPM and SQUID, a statistical test of equivalence (two one-sided tests procedure) has been performed. Below, statistical distribution of M100 latencies across all trials is represented with box plots for SQUID and OPM respectively (Fig 11). Considering a mean difference of 1.5 ms between OPM and SQUID M100 latencies (effect size of 0.5), the equivalence test revealed that M100 latencies distributions were statistically equivalent and not different between OPM and SQUID measurements (p=0.02).

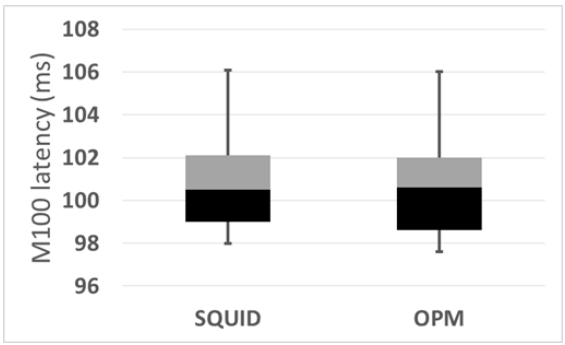

Fig. 11. Box plots from the study of the M100 peaks latencies obtained through all the sessions.

Moreover, we have compared the pattern of the auditory evoked brain response between OPM and the reference SQUID magnetometer over the entire time window (Spearman correlation). Results showed that OPM signals were correlated to SQUID signals with a correlation of 0.69.

These results confirm that our vectorial ^{4}He OPM sensors can reliably detect AEF signals with a latency and a morphology which are statistically similar to reference SQUIDs data.

2) Visual evoked fields VEF

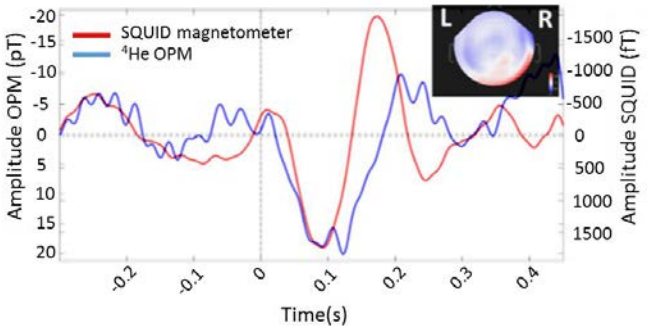

Fig. 12. Averaged VEF: Topography of VEF as recorded in MEG with the averaged signal over 35 epochs obtained from one SQUID sensor magnetometer) placed in the right occipital area and averaged signals over 28 epochs obtained from our OPMs sensor.

Considering M100 brain response to visual stimuli, figure 12 displays averaged curves obtained from one SQUID and the VEF topography at 94.7 ms (M100 peak). The corresponding VEF from OPM sensor placed over occipital region, averaged across 28 trials, appears noisier. However, a M100 response could be obviously observed at the same latency compared to SQUID with a peak value of 20 pT, as compared to 1.7 pT for SQUID. This difference is likely to be due to the closer distance between the OPM and the scalp.

As only one session was available for VEF, no statistical test should be done to compare latency distribution between OPM and SQUID.

3) Induced alpha activity measured by the OPMs

Figure shows the normalized power (z score) in the alpha frequency band 8-12 Hz. From SQUID recording, a modulation (power decrease between the closed eyes and open eyes conditions) of the normalized power in the alpha frequency band can be observed when the subject opens his eyes (at t = 0 s) (Fig 14a). This is obviously displayed on the time-course of the averaged power in the alpha frequency band (green curve). A similar power decrease in alpha frequency band was revealed from OPM recordings (Fig 14b). The time course of averaged power in the alpha band (green curve) is consistent with SQUID data. This result provides evidence that it is possible to record a brain activity modulation induced by eyes opening with our OPM in addition to evoked activities described above.

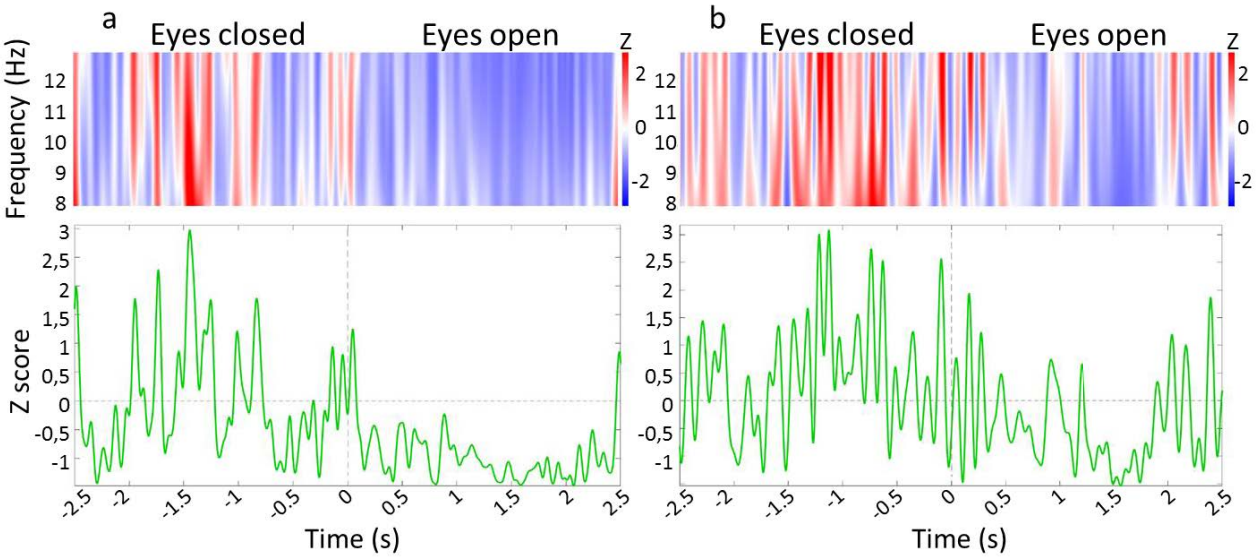

Fig. 13. Normalized (Z-score) time-frequency maps between 8 and 12 Hz (alpha band) in the top of the figure for SQUID (a) and OPMs (b) and corresponding time courses of the normalized power in the bottom of the figure. The average has been obtained over all the sessions, i.e. 16 eyes opening for SQUID and 14 for OPM.

V. Discussion

In this study, OPM measurements are cross-validated by SQUID recordings: pattern and latency are the main criteria of assessment for the comparison. Phantom and healthy subject measurements have demonstrated the possibility to detect MEG signal of interest at room-temperature with a parametric vector ^{4}He OPM in clinical conditions and without increasing the recording time. This has been done for evoked fields as well as induced brain activity, namely the alpha power modulation induced by eyes opening.

It is worth mentioning that OPM and SQUID signals slightly differ for two reasons.

The first difference comes from interferences rejection approaches. For the OPM, the MEG signal of interest is recorded by only one sensor and denoised with a reference sensor placed away from any brain magnetic field sources and in the present paper, by using ICA.

For SQUIDs, recordings were done with all sensors (306 sensors covering the head) and post-processed with SSS. The SSS algorithm takes advantage of the generous spatial oversampling of both biomagnetic and external disturbance magnetic fields, as provided by current multi-channels MEG machines [44]. Signal space separation is a purely spatial method to transform electromagnetic multichannel data into uncorrelated basic components, e.g. magnetic multipole moments [51] [52]. With SSS, it is possible to uniquely estimate the multipoles separately for the signals arising from the internal and external volumes of the sensor array. Therefore, the denoised brain magnetic field corresponding to SSS-processed SQUID signal is a reconstruction based on the estimated multipoles arising from inside of the sensor helmet, excluding those arising from outside.

This should explain variability between OPM and SQUID signals which are not strictly similar as it can be observed on the figures and as revealed by Spearman correlations reported in this study. However, the use of SSS algorithm was mandatory as the MaxShield® active compensation required for recordings induces cross-talk. This cross talk is also corrected by applying SSS algorithm.

The second difference comes from spatial location of both sensors: the chosen SQUID, which is located in the area of interest, may not be exactly in the same spatial location as OPM_1.

These two elements can explain why evoked fields patterns recorded by OPM and SQUIDs can be slightly different whereas the M100 latencies are very close between SQUIDs and OPMs. This is notably true for the visual evoked field for which averaged OPM signal is somewhat noisier. The lower number of trials available for averaging in the visual modality could also explain why averaged signal is noisier and why a lower Spearman correlation level was obtained.

Interestingly, we also show that our OPM sensor is able to record induced brain activity, which is time locked to a stimulus but not phase locked. Patterns obtained from Time Frequency analysis in the alpha band are very similar between SQUID and OPM and time series of the averaged alpha band power well revealed the decrease of power related to eyes opening.

An important observation of this cross-validation concerns the amplitude of signals recorded with OPM compared to SQUIDs. Even if our sensor is, in its current development stage, less sensitive than the SQUIDs, the impact on the signal

to noise ratio is partly compensated by the higher amplitude of the signal recorded by the OPM. Indeed, as our OPMs don't require thermal insulation system, the distance between the sensor and the subject can be reduced resulting in an increase of the amplitude of the MEG signal. The distance between the ^{4}He cell, the sensitive element of our OPM, and the subject's scalp is estimated to 5 mm (measured from cell wall) against around 30 mm for the SQUIDs (based on technical configuration of Elekta Vectorview Neuromag 306® MEG machine). As observed on the auditory and visual evoked field's curves, the scale for OPM is expressed in 10^3 fT versus a scale in fT for SQUID. Based on these first results, the multiply factor of signal amplitude should be estimated to 5 from AEF curves and 10 for VEF ones. This result well agrees with a recent work [53] quantifying the improvement in recording MEG with simulated on-scalp OPM arrays compared to a 306-channels SQUID array such as Vectorview Neuromag MEG machine used in our study. This work reported, that OPM yielded 7.5 times higher signal power compared to the SQUID magnetometers. This estimation was performed for a simulated 102 channels OPMs array in which OPMs were normal to the scalp surface as in our experimental setup, excepted we only had one OPM sensor over the head. Another work based on real SQUIDs and alkali OPM measurements [32] also compared signal amplitude between both kinds of magnetometers, based on somatosensory evoked fields. Authors reported that signal recorded with one OPM sensor (similar to the one described in [54]) was 15 higher than one measured with the SQUIDs. Therefore, our observation, even if this needs to be more investigated and precisely quantified, is in line with previous data reported in the literature. This shows the potential of the ^{4}He OPM sensor for biomagnetic imaging applications, notably by considering that sensitivity of our sensor is currently improved by reducing laser noise.

VI. Conclusion

In this paper, we have presented preliminary proofs of concepts concerning the possibility to record MEG signals with parametric vector ^{4}He magnetometers in a clinical environment. For this purpose, two MEG experiments were carried out with a brain phantom as well as with a healthy subject. Both evoked and induced activities have been successfully recorded. Data recorded with the OPMs were cross-validated with SQUIDs measurements. Similar latencies and patterns have been obtained with OPMs and SQUIDs. Moreover, as the sensor works at room-temperature, the distance between the sensor and the scalp is significantly reduced resulting in higher signal amplitudes.

Further work will concentrate on improving the sensitivity of the ^{4}He OPM by implementing new detection methods and reducing the noise of the pump laser. An ultra-low noise 1083 nm laser diode is currently developed and sensor noise reduction evaluation is ongoing. Also, bandwidth can be easily extended to 2 kHz as ^{4}He OPM doesn't suffer from the same limitations encountered with alkali OPM. Furthermore, an array configuration is under development dedicated to multi-channels recordings. The array is required for neuroscientific research and clinical purposes.

VII. Acknowledgment

This work was supported by the French National Research Agency (ANR) through Carnot funding. The authors are grateful to Pr Xavier De Tiège (ULB-Hospital Erasme, Brussels, Belgium) for his valuable comments and scientific support; to C Sandre-Ballester from the Innovation and Clinical Research Department at Grenoble Medical University Hospital; to the medical team (Grenoble Medical University Hospital) assisting us in this clinical trial; to L. Parkkonen for his recommendations on the Elekta Phantom and to F. Tadel for his advice for data analysis with Brainstorm®.

VIII. References

[1] PC Hansen,ML Kringelbach, R Salmelin. MEG: An introduction to methods. Publisher: Oxford University Press USA. June 2010 ISBN: 0195307232.

[2] S. Almubarak, A. Alexopoulos, F. Von-Podewils, I. Wang, Y. Kakisaka, J. Mosher, J. Bulacio, J. Gonzalez-Martinez, W. Bingaman, and R. Burgess, "The correlation of magnetoencephalography to intracranial EEG in localizing the epileptogenic zone: A study of the surgical resection outcome," Epilepsy Res., vol. 108, no. 9, pp. 1581–1590, Nov. 2014.

[3] R. Knowlton, R. Elgavish, J. Howell, J. Blount, J. Burneo, E. Faught, P. Kankirawatana, K. Riley, R. Morawetz, J. Worthington, and R. Kuzniecky, "Magnetic Source Imaging versus Intracranial Electroencephalogram in Epilepsy Surgery: A prospective Study," Ann. Neurol., vol. 59, no. 5, pp. 835–842, Apr. 2006.

[4] H. Stefan, C. Hummel, G. Scheler, A. Genow, K. Druschky, C. Tilz, M. Kaltenhäuser, R. Hopfengärtner, M. Buchfelder, and J. Romstöck, "Magnetic brain source imaging of focal epileptic activity: a synopsis of 455 cases," Brain, vol. 126, pp. 2396–2405, Jun. 2003.

[5] Jmail N, Gavaret M, Bartolomei F, Chauvel P, Badier JM, Bénar CG. Comparison of Brain Networks During Interictal Oscillations and Spikes on Magnetoencephalography and Intracerebral EEG. Brain Topogr. 2016 Sep;29(5):752-65. doi: 10.1007/s10548-016-0501-7. Epub 2016 Jun 22.

[6] Jayabal V, Pillai A, Sinha S, Mariyappa N, Satishchandra P, Gopinath S, Radhakrishnan K. Role of magnetoencephalography and stereo-electroencephalography in the presurgical evaluation in patients with drug-resistant epilepsy. Neurol India. 2017;65(Supplement):S34-S44. Review.

[7] De Tiège X, Lundqvist D, Beniczky S, Seri S, Paetau R. Current clinical magnetoencephalography practice across Europe: Are we closer to use MEG as an established clinical tool? Seizure. 2017 Jun 8;50:53-59.

[8] D. Rudrauf, O. David, J. Lachaux, C. Kovach, J. Martinerie, B. Renault, and A. Damasio, "Rapid Interactions between the Ventral Visual Stream and Emotion-Related Structures Rely on a Two-Pathway

Architecture," J Neurosci, vol. 28, no. 11, pp. 2793–2803, Mar. 2008.

[9] J. R. King, F. Faugeras, A. Gramfort, A. Schurger, I. El Karoui, J. D. Sitt, B. Rohaut, C. Wacongne, E. Labyt, T. Bekinschtein, L. Cohen, L. Naccache, and S. Dehaene, "Single-trial decoding of auditory novelty responses facilitates the detection of residual consciousness," NeuroImage, vol. 83, pp. 726–738, 2013.

[10] C. Wacongne, E. Labyt, V. van Wassenhove, T. Bekinschtein, L. Naccache, and S. Dehaene, "Evidence for a hierarchy of predictions and prediction errors in human cortex," PNAS, vol. 108, no. 51, pp. 20754–20759, 2011.

[11] P. Rahkonen, P. Nevalainen, L. Lauronen, E. Pihko, A. Lano, S. Vanhatalo, A.-K. Pesonen, K. Heinonen, K. Räikkönen, L. Valanne, T. Autti, S. Andersson, and M. Metsäranta, "Cortical somatosensory processing measured by magnetoencephalography predicts neurodevelopment in extremely low-gestational-age infants," Pediatr. Res., vol. 73, no. 6, pp. 763–771, Jun. 2013.

[12] Maestu F, Pena JM, Garces P, Gonzalez S, Bajo R, Bagic A, et al. A multicenter study of the early detection of synaptic dysfunction in Mild Cognitive Impairment using Magnetoencephalography derived functional connectivity. Neuroimage Clin. 2015;9:103-9.

[13] Engels MM, Hillebrand A, van der Flier WM, Stam CJ, Scheltens P, van Straaten EC. Slowing of Hippocampal Activity Correlates with Cognitive Decline in Early Onset Alzheimer's Disease. An MEG Study with Virtual Electrodes. Front Hum Neurosci. 2016;10:238.

[14] Lopez-Sanz D, Bruna R, Garces P, Camara C, Serrano N, Rodriguez-Rojo IC, et al. Alpha band disruption in the AD-continuum starts in the Subjective Cognitive Decline stage: a MEG study. Scientific reports. 2016;6:37685.

[15] Fernandez A, Turrero A, Zuluaga P, Gil-Gregorio P, del Pozo F, Maestu F, et al. MEG delta mapping along the healthy aging-Alzheimer's disease continuum: diagnostic implications. J Alzheimers Dis. 2013;35(3):495-507.

[16] Boon LI, Hillebrand A, Olde Dubbelink KTE, Stam CJ, Berendse HW. Changes in resting-state directed connectivity in cortico-subcortical networks correlate with cognitive function in Parkinson's disease. Clin Neurophysiol. 2017 Jul;128(7):1319-1326.

[17] Bosboom JL, Berendse HW, Hillebrand A. A three dimensional anatomical view of oscillatory resting-state activity and functional connectivity in Parkinson's disease related dementia: An MEG study using atlas-based beamforming. Neuroimage Clin. 2012 Nov 17;2:95-102.

[18] Heinrichs-Graham E, Wilson TW, Santamaria PM, Heithoff SK, Torres-Russotto D, Hutter-Saunders JA, Estes KA, Meza JL, Mosley RL, Gendelman HE. Neuromagnetic evidence of abnormal movement-related beta desynchronization in Parkinson's disease. Cereb Cortex. 2014 Oct;24(10):2669-78. doi: 10.1093/cercor/bht121. Epub 2013 May 3.

[19] Rowland JA, Stapleton-Kotloski JR, Alberto GE, Rawley JA, Kotloski RJ, Taber KH, Godwin DW. Contrasting Effects of Posttraumatic Stress Disorder and Mild Traumatic Brain Injury on the Whole-Brain Resting State Network: A Magnetoencephalography Study. Brain Connect. 2017 Feb;7(1):45-57.

[20] Alhourani A, Wozny TA, Krishnaswamy D, Pathak S, Walls SA, Ghuman AS, Krieger DN, Okonkwo DO, Richardson RM, Niranjan A. Magnetoencephalography-based identification of functional connectivity network disruption following mild traumatic brain injury. J Neurophysiol. 2016 Oct 1;116(4):1840-1847.

[21] Vakorin VA, Doesburg SM, da Costa L, Jetly R, Pang EW, Taylor MJ. Detecting Mild Traumatic Brain Injury Using Resting State Magnetoencephalographic Connectivity. PLoS Comput Biol. 2016 Dec 1;12(12).

[22] Tewarie P, Schoonheim MM, Stam CJ, van der Meer ML, van Dijk BW, Barkhof F, Polman CH, Hillebrand A. Cognitive and clinical dysfunction, altered MEG resting-state networks and thalamic atrophy in multiple sclerosis. PLoS One. 2013 Jul 31;8(7):e69318. doi: 10.1371/journal.pone.0069318. Print 2013.

[23] Tewarie P, Hillebrand A, Schoonheim MM, van Dijk BW, Geurts JJ, Barkhof F, Polman CH, Stam CJ. Functional brain network analysis using minimum spanning trees in Multiple Sclerosis: an MEG source-space study. Neuroimage. 2014 Mar;88:308-18. doi: 10.1016/j.neuroimage.2013.10.022. Epub 2013 Oct 22.

[24] Tewarie P, Schoonheim MM, Schouten DI, Polman CH, Balk LJ, Uitdehaag BM, Geurts JJ, Hillebrand A, Barkhof F, Stam CJ. Functional brain networks: linking thalamic atrophy to clinical disability in multiple sclerosis, a multimodal fMRI and MEG study. Hum Brain Mapp. 2015 Feb;36(2):603-18. doi: 10.1002/hbm.22650. Epub 2014 Oct 8.

[25] T. Sander, J. Preusser, R. Mhaskar, J. Kitching, L. Trahms, et S. Knappe, « Magnetoencephalography with a chip-scale atomic magnetometer », Biomed. Opt. Express, vol. 3, no 5, p. 981‑990, 2012

[26] K. Kim, S. Begus, H. Xia, S. Lee, V. Jazbinsek, Z. Trontelj, and M. Romalis, "Multi-channel atomic magnetometer for magnetoencephalography: A configuration study," NeuroImage, vol. 89, pp. 143–151, Apr. 2014.

[27] K. Kamada, K, D. Sato, Y. Ito, H. Natsukawa, K. Okano, N. Mizutani, and T. Kobayashi, "Human magnetoencephalogram measurements using newly developed compact module of high-sensitivity atomic magnetometer," Jpn. J. Appl. Phys., vol. 54, no. 2, p. 026601, 2015.

[28] Boto E, Meyer SS, Shah V, Alem O, Knappe S, Kruger P, Fromhold TM, Lim M, Glover PM, Morris PG, Bowtell R, Barnes GR, Brookes MJ. A new generation of magnetoencephalography: Room temperature

measurements using optically-pumped magnetometers. Neuroimage. Apr 1; 149:404-414, 2017

[29] V. K. Shah and R. T. Wakai, "A compact, high performance atomic magnetometer for biomedical applications," Phys. Med. Biol. 58(22), 8153–8161, 2013

[30] C. Johnson, P. D. D. Schwindt, and M. Weisend, "Magnetoencephalography with a two-color pump-probe, fibercoupled atomic magnetometer," Appl. Phys. Lett. 97(24), 28, (2010).

[31] C. Johnson and P. D. D. Schwindt, "A two-color pump probe atomic magnetometer for magnetoencephalography," Proc. IEEE Int. Freq. Cont., 29, 371–375, (2010)

[32] C. N. Johnson, P. D. D. Schwindt, and M. Weisend, "Multi-sensor magnetoencephalography with atomic magnetometers," Phys. Med. Biol. 58(17), 6065–6077 (2013).

[33] S. Knappe, T. Sander, and L. Trahms, "Optically-Pumped Magnetometers for MEG," in S. Supek and C.J. Aine (eds.), Magnetoencephalography, Springer-Verlag Berlin Heidelberg 2014, pp. 993–999 DOI: 10.1007/978-3-642-33045-2_49,

[34] Savukov I, Boshier MG. A High-Sensitivity Tunable Two-Beam Fiber-Coupled High-Density Magnetometer with Laser Heating. Sensors (Basel). 2016 Oct 13;16(10). pii: E1691.

[35] Colombo AP, Carter TR, Borna A, Jau YY, Johnson CN, Dagel AL, Schwindt PD. Four-channel optically pumped atomic magnetometer for magnetoencephalography. Opt Express. 2016 Jul 11;24(14):15403-16. doi: 10.1364/OE.24.015403.

[36] Morales S, Corsi MC, Fourcault W, Bertrand F, Cauffet G, Gobbo C, Alcouffe F, Lenouvel F, Le Prado M, Berger F, Vanzetto G, Labyt E. Magnetocardiography measurements with 4He vector optically pumped magnetometers at room temperature. Phys Med Biol. 2017 Mar 3. doi: 10.1088/1361-6560/aa6459.

[37] J. Dupont-Roc, "Etude théorique de diverses résonances observables en champ nul sur des atomes 'habillés' par des photons de radiofréquences," J. Phys., vol. 32, no. 2–3, pp. 135–144, 1971.

[38] J. Léger, "Magnétométrie à pompage optique: conception, réalisation, et évaluation des performances et évaluation des performances d'un magnétomètre scalaire utilisant l'Hélium 4 pompé par un laser LNA," Thèse, Université Joseph Fourier, Grenoble, 1990. http://www.theses.fr/1990GRE10064

[39] M. Le Prado, " Conception, réalisation et application d'un magnétomètre atomique vectoriel," Thèse, Université de Franche Comté, 2014. http://www.theses.fr/2014BESA2003

[40] J. Dupont-Roc, "Détermination par des méthodes optiques des trois composantes d'un champ magnétique très faible," Rev. Phys. Appliquée, vol. 5, no. 6, pp. 853–864, Dec. 1970.

[41] C. Cohen-Tannoudji, J. Dupont-Roc, S. Haroche, and F. Laloë, "Diverses résonances de croisement de niveaux sur des atomes pompés optiquement en champ nul I. Théorie," Rev. Phys. Appliquée, vol. 5, no. 1, pp. 95–101, Feb. 1970.

[42] C. Cohen-Tannoudji, J. Dupont-Roc, S. Haroche, and F. Laloë, "Diverses résonances de croisement de niveaux sur des atomes pompés optiquement en champ nul II. Applications à la mesure de champs faibles," Rev. Phys. Appliquée, vol. 5, no. 1, pp. 102–108, Feb. 1970.

[43] D Oyama, , Y Adachi, M Yumoto, I Hashimoto, G Uehara. Dry phantom for magnetoencephalography — Configuration, calibration, and contribution. J Neurosci Meth Vol 251, 24-36, Aug 2015.

[44] S. Taulu, M. Kajola, and J. Simola, "The Signal Space Separation method," Biomed Tech, vol. 48, 2004.

[45] F. Tadel, S. Baillet, J. C. Mosher, D. Pantazis, and R. M. Leahy, "Brainstorm: A User-Firendly Application for MEG/EEG Analysis," Comput. Intell. Neurosci., vol. 2011, Jan. 2011.

[46] A. Hyvärinen, "New Approximations of Differential Entropy for Independent Component Analysis and Projection Pursuit," Adv. Neural Inf. Process. Syst., pp. 273–279, 1998.

[47] A. Hyvärinen and E. Oja, "Independent Component Analysis: Algorithms and Applications," Neural Netw., vol. 13, no. 4–5, pp. 411–430, 2000.

[48] T. Sander, TH, G. Wübbeler, A. Lueschow, G. Curio, and L. Trahms, "Cardiac Artifact Subspace Identification and Elimination in Cognitive MEG Data Using Time-Delayed Decorrelation," Biomed. Eng. IEEE Trans. On, vol. 49, no. 4, pp. 345–354, 2002.

[49] D. Mantini, R. Franciotti, G. Romani, and V. Pizzella, "Improving MEG source localizations: An automated method for complete artifact removal based on independent component analysis," NeuroImage, vol. 40, no. 1, pp. 160–173, 2008.

[50] Lakens D. Equivalence Tests: A Practical Primer for *t* Tests, Correlations, and Meta-Analyses. May;8(4):355-362, 2017

[51] Taulu S and Kajola M 2005 Presentation of electromagnetic multichannel data: the signal space separation method J. Appl. Phys. 97 124905

[52] Taulu S, Simola J and Kajola M 2005 Applications of the signal space separation method IEEE Trans. Signal Process. 53 3359

[53] Iivanainen J, Stenroos M, Parkkonen L.Measuring MEG closer to the brain: Performance of on-scalp sensor arrays. Neuroimage. 2017 Feb 15;147:542-553. doi: 10.1016/j.neuroimage.2016.12.048. Epub 2016 Dec 19.

[54] S. Knappe, T. H. Sander, O. Kosch, F. Wiekhorst, J. Kitching, and L. Trahms, "Cross-validation of microfabricated atomic magnetometers with superconducting quantum interference devices for biomagnetic applications," Appl. Phys. Lett. 97(13), 133703 (2010).